Optica Applicata, Vol. LIV, No. 2, 2024
DOI: 10.37190/oa240209

Improving the ozone retrieval accuracy by minimizing the asynchronous offset in differential absorption lidar systems

DULIANG ZHAO[1,2], CHAO TANG[3], XIANGRUI MENG[1], SHILI LI[1,2], YANFEI WANG[1,2], ZHENGTING DU[2,4], LONGBAO YU[1,2], SHAN JIANG[1,2,*]

[1]Universities Joint Key Laboratory of Photoelectric Detection Science and Technology in Anhui Province, Hefei normal university, Hefei, 230601, China

[2]School of Physics and Materials Engineering, Hefei Normal University, Hefei 230601, China

[3]School of Electronic Information and Integrated Circuit, Hefei Normal University, Hefei 230601, China

[4]Information Materials and Intelligent Sensing Laboratory of Anhui Province, Anhui University, Hefei 230601, China

[*]Corresponding author: sjiang@hfnu.edu.cn

The differential absorption lidar (DIAL) has been proposed as an effective method for detecting ozone in the atmosphere. An important factor affecting its detecting precision is the asynchronous offset between backscattered signals at different wavelengths. Recently, a DIAL was built by our group, and the impact of the asynchronous offset was tested and studied. The simulation results show that the measurement error caused by the offset is negatively correlated with the altitude. Meanwhile, the offset has an additional effect in areas with sharp ozone concentration changes. Comparative experiments were carried out by our DIAL system and an airborne atmospheric monitoring system in the Nanjing test site. The results show that a 15 m offset in DIAL led to serious errors in retrieval results. These errors are inversely related to the detection altitude and reach up to 13 ppb, which is consistent with the results from simulations. After controlling the relative position of the backscattered signal to minimize the asynchronous offset, the maximum error was reduced to 2 ppb. Then the optimized DIAL was used for 48-hour continuous observation with a proven ozone analyzer. It shows that the optimized DIAL has high detecting accuracy and stability as point-fixed instruments.

Keywords: lidar, differential absorption, asynchronous offset, ozone.

1. Introduction

Ozone is one of the most important trace gas in the atmosphere. The ozone layer in the stratosphere protects life by absorbing ultraviolet radiation from the sun. However,

excessive ozone near the ground can harm human health and plant growth. In recent years, as PM2.5 and VOCs concentrations have decreased, ozone has become one of the major pollutants in China. Therefore, it is important to detect surface ozone with high precision, which can provide sufficient data for understanding the interaction between surface and upper-altitude air, validating satellite retrievals, and evaluating air-quality models [1,2].

DIAL system is suitable for long-term ozone monitoring as a complement to satellite and ozonesonde measurements [3,4]. However, its detecting accuracy can be affected by many factors, such as the absorption of other gases (*i.e.* NO_2, SO_2, O_2), the interference of aerosols, and the extraction of backscattered signals from noise [5-6]. A multiwavelength lidar system, using either Rayleigh/Mie signals or the Raman nitrogen signal, has been discussed and verified as a way to efficiently correct the ozone measurements from the systematic bias due to aerosol and other gases [7,8]. Then, a Fernald-DIAL algorithm in these systems was introduced to retrieve ozone concentration and extinction coefficient simultaneously and reduce the impact [6]. In addition, optimizing the power ratio of two emitted lights and reducing the spatial resolution can also suppress the noise floor and improve the retrieval accuracy of ozone concentration [6,9].

Furthermore, the DIAL technique is very sensitive to asynchronous offset in the time domain [10]. DIAL system has two detecting wavelengths. The first data point of backscattered signal for each wavelength should corresponds to the same reference altitude, so the following data points can have one-to-one correspondence in altitude [11]. However, several factors break this correspondence and lead to an asynchronous offset (*i.e.* the time delay between the trigger of the photodiode and the data acquisition card, the internal delay in the different channels of the function generator, and the internal delay in the data acquisition card [10-14]). KUANG *et al*. found that when the offset is greater than 0.5 m, the retrieval errors are unacceptable (>10%) below 200 m. FERNANDO *et al*. revealed that an overestimation of about 0.5×1018 m−3 can be introduced, which led to a 50% error at 100 m, for the offset observed between the two transient recorders (23 ns or 3.45 m) [11]. In previous publications, few reports have been noted on the asynchronous offset in the DIAL system.

This paper describes an optimization by minimizing the asynchronous offset to improve the performance of DIAL. The structure of this paper is as follows: in Section 2, the DIAL structure and work principles are described; in Section 3, we analyzed the effect of the asynchronous offset on the ozone retrieval accuracy; in Section 4, we have improved our DIAL and carried out comparative experiments to verify its performance; in Section 5, a summary of the key achievements and an outlook for future are presented.

2. Materials and methods

In the DIAL system, a laser emitting at 266 nm with a pulse energy of 50 mJ operates at a 20 Hz repetition rate. The laser light is then divided into two beams, each carrying

T a b l e 1. Key parameters of the DIAL.

Transmitter	
Emitting wavelengths	289 nm/299 nm
Output energy	10 mJ@289, 8 mJ@299
Divergence angle	0.2 mrad
Receiver	
Telescope aperture	300 mm
Telescope focal length	1.2 m
Stop	0.3 mm
Distance between receiving and emitting axes	0.2 m
System specifications	
Sampling rate of the acquisition card	40 MHz
Temporal resolution	Adjustable (5 min, 10 min, 15 min, 20 min)
Detection range	From 0.05 to 3 km

equal energy. Each beam is then focused into a Raman cell, 1.2 meters long, capped with sapphire windows. One cell is filled with D2 at a pressure of 3200 kPa, shifting the wavelength from 266 to 289 nm. The other cell contains H2 at 3500 kPa, altering the wavelength from 266 to 299 nm. After collimation and expansion, both beams pass through the cells and are then transmitted into the atmosphere.

Turning mirrors are mounted on motor-controlled holders, enabling beam alignment. The receiver, a Cassegrain telescope with a 1.2 m focal length, collects the backscattered light. A dichroic lens reflects the 289 nm backscattered signal and transmits the 299 nm signal. To suppress solar noise, a narrowband interference filter with a 1.0 nm full-width half maximum is used. Each light beam is focused into its respective photomultiplier tube (PMT). A stop is placed in the focal plane to narrow the field of view [15]. Table 1 presents the DIAL system's key parameters.

In DIAL technology, we can use the λ_{ON} to denote the strong absorbing wavelength and the λ_{OFF} to denote the weak absorbing wavelength. By applying the Lidar equation [16-17], we obtain the ozone number density N_{O_3}, as follows:

$$N_{O_3}(z) = \frac{1}{\Delta\sigma_{O_3}} \left\{ \frac{\partial}{\partial z}\left[\ln\frac{P_{OFF}(z)}{P_{ON}(z)}\right] - \Delta\sigma_M N_a(z) - \left[\sum\nolimits_{ig} \Delta\sigma_{ig}(z) N_{ig}(z)\right] - \Delta\alpha_P(z) + \Lambda\beta(z) + \Lambda\eta(z) + \Lambda Z(z) \right\} \quad (1)$$

where, $\Delta\sigma_{O_3}$ and $\Delta\sigma_M$ are the difference of ozone absorption cross-section and molecular cross section in λ_{ON} and λ_{OFF}, P_{ON} and P_{OFF} are the power of backscattered signal converted by each PMT, N_a is the air number density, $\Delta\sigma_{ig}$ and N_{ig} are the differential absorption cross section and number density of other absorbing molecules besides ozone, $\Lambda\beta$ is the difference of the atmospheric backscattered coefficient in λ_{ON} and λ_{OFF},

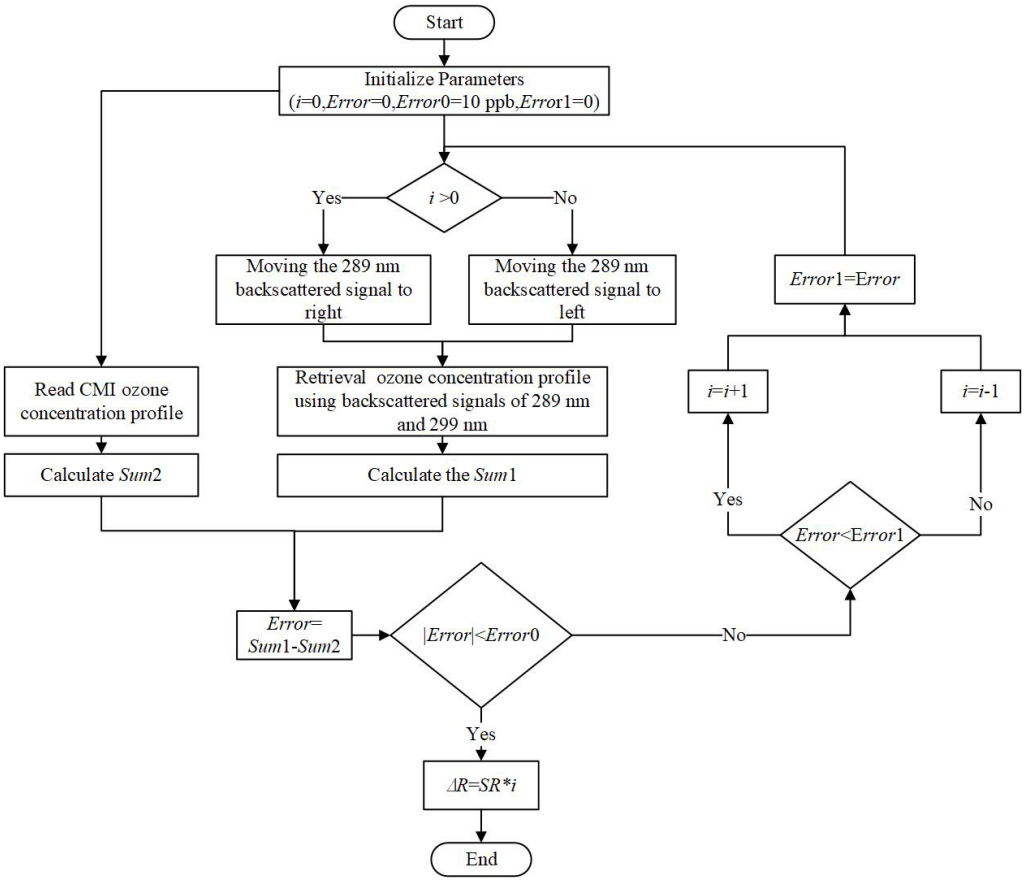

Fig. 1. The method for determination of asynchronous offset.

$\Lambda\eta$ represents the difference in efficiency of both receivers and ΛZ is synchronization difference between each channels.

ΔR, called asynchronous offset in this paper, is the main contribution of ΛZ. It is the shift in meters of the ON channel with respect to the OFF channel for backscattered signal. ΔR is an integer multiple of the spatial resolution (SR) which depends on the sampling rate of the acquisition card (SRAC). In our DIAL system, the SRAC is 40 MHz, so the SR is 7.5 m. The asynchronous offset can be reduced by adjusting the relative position of the data points between two backscattered signals at different wavelength. In practice, the determination of offset, which can be obtained through the method as shown in Fig. 1, is related to the bias for DIAL and the calibrated measuring instrument (CMI).

In Fig. 1, an iteration is executed to find the system asynchronous offset depending on the bias between DIAL and CMI. This iteration involves three variables (i, Error1 and Error) and a settable constant(Error0), which are initialized at the beginning. The variable i determines the direction in which the 289 nm signal moves. A negative i indicates

that the 289 nm backscattered signal should be moved to the right, while a positive i indicates that the 289 nm signal should be moved to the left. The ozone concentration profile is retrieved by using the moved 289 nm signal and the original 299 nm signal. Sum1 and Sum2 are the averages of the ozone profile in the range 50 to 1000 m for Lidar and CMI,respectively. Their difference is calculated and passed to error. If an error is less than Error0, the iteration is completed and the value of asynchronous offset is obtained by SR·i. Otherwise, error and Error1 are compared for further iteration. i is updated based on the comparison and Error1 is updated by Error, which will participate in the next iteration.

ΔR has a great impact on ΛZ. Hence, the study of ΔR is important for improving detection accuracy in DIAL.

3. Simulation and analysis

We simulated and analyzed the effect of ΔR with the system parameters. The total atmospheric scattering and extinction coefficient were obtained from the 1976 U.S. Standard Atmosphere [18]. The different values of ΔR were selected by the integer multiples of 7.5 m. The raw signals converted by the photodetector at detection wavelengths were calculated based on the parameters in Table 1, the Lidar equation, and a reference ozone profile with 50 ppb at all altitudes. The ΔR is introduced to control the asynchronous offset between the raw signals. The calculated ozone profile was retrieved based on Eq. (1).

3.1. The effect of asynchronous offset on same ozone concentrations

In Fig. 2, eight revised ozone profiles were retrieved with different ΔR values (7.5, 15, 22.5, and 30 m) that were introduced into the 289 nm signal and 299 nm signal sep-

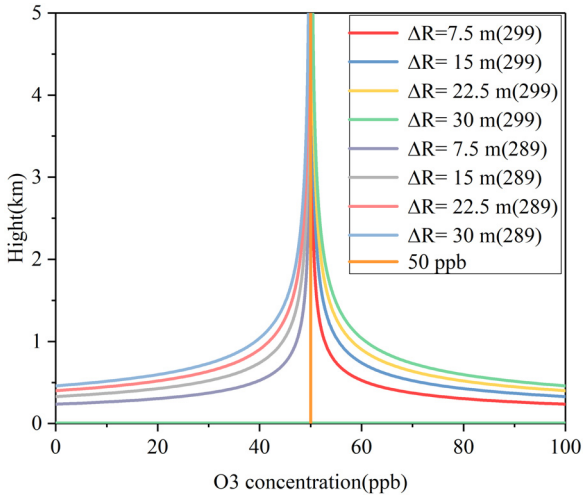

Fig. 2. Ozone concentration profiles at different ΔR.

arately. The reference ozone profile with 50 ppb at all altitudes was also plotted for comparison and analysis.

The results show that: *i*) In the 289 nm/299 nm DIAL system if there is an offset in the 299 nm signal, the obtained ozone concentration will be higher than the reference ozone concentration. Conversely, if there is an offset in the 289 nm signal, the concentration will be lower than 50 ppb. *ii*) Under the same altitude, the larger the ΔR, the more the retrieval results deviate from the reference profile. *iii*) For the same ΔR, the retrieval error has an exponentially decaying relationship with the measurement altitude. Away from the laser emitter, the retrieval error decreases rapidly, and the retrieval result quickly approaches the reference profile. The results show that increasing ΔR leads to larger errors in ozone retrieval.

3.2. The effect of asynchronous offset on different ozone concentrations

The following section investigates the relationship between ozone concentration and retrieval accuracy under the same ΔR in the DIAL system.

The reference ozone concentration profile was reconstructed with the following steps: a uniform ozone concentration of 50 ppb was assumed from 0 to 750 m. From 750 to 787.5 m, a rapid increase in ozone concentration at a rate of 5 ppb/m was set. The high ozone area ranged from 787.5 to 862.5 m, with ozone uniformly distributed at 75 ppb. From 862.5 to 937.5 m, the ozone concentration was assumed to decrease rapidly at a rate of 5 ppb/m, eventually returning to a concentration of 50 ppb from 937.5 to 5000 m.

Based on the reconstructed ozone concentration profile, the raw signals in the 289 nm/299 nm DIAL system are calculated. The value of ΔR is selected as 15 m to retrieve the ozone concentration with offset at 299 nm. Figure 3 shows the effect of ΔR on DIAL for different ozone concentrations.

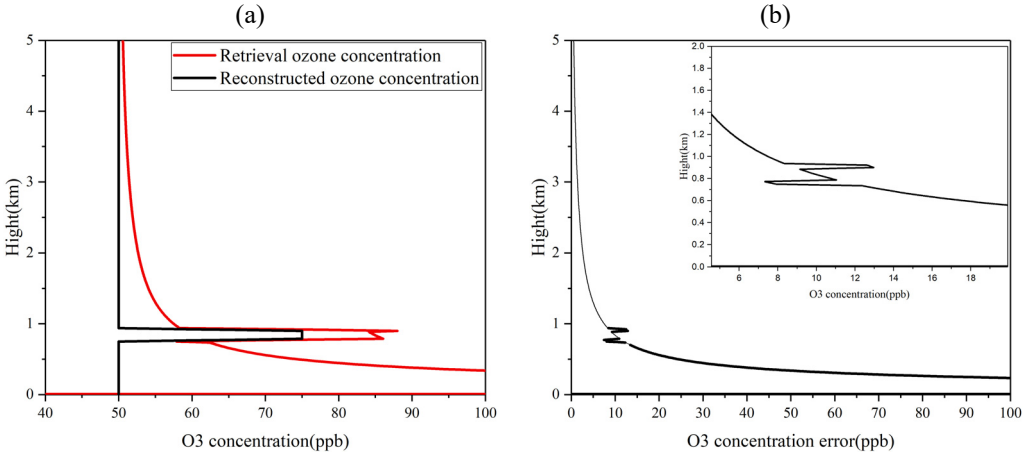

Fig. 3. Effect of ΔR on DIAL for different ozone concentrations. (a) The reconstructed and retrieval ozone concentration profiles. (b) Retrieval error curve.

In Fig. 3(a), the black curve shows the reconstructed ozone concentration profile, while the red curve depicts the profile retrieved after introducing ΔR. Figure 3(b) displays the error curve for both profiles. Calculations reveal that: *i*) The offset similarly affects ozone retrieval accuracy in both high and low concentration areas, with comparable impacts at 50 and 75 ppb. *ii*) The offset significantly influences areas with abrupt ozone concentration changes, adding an error to the retrieval result during transitions from low to high concentrations, evident in Fig. 3(b)'s peak. This deviation increases the overall error for transitions from low to high concentrations, while transitions from high to low result in a decreased overall error. *iii*) The additional error directly correlates with the ozone concentration change rate.

Calculations show that the ΔR affects the boundary region of high ozone values. Specifically, the overall error increases in the rising boundary region due to the generation of additional errors and decreases in the falling boundary region.

It can be seen that the offset can affect the measurement accuracy of the DIAL system obviously. In particular, the effect is more pronounced in regions with lower detection altitudes. If this offset is not minimized, the performance of DIAL will seriously degrade. Continuous field observations are carried out for the DIAL system to confirm the theoretical analyses and ensure the higher detection accuracy and reliability of the equipment by an optimization method.

4. Experiments and discussion

The experiments were performed on 12th, 20th, and 21th–23th May 2022 at the playground of the Xianlin Campus of Nanjing University (118°57′10″ E, 32°06′57″ N). The weather during the experiment was mostly cloudy, with winds mainly from the southeast and northwest. The temperature ranged from 20 to 31°C, and the average relative humidity was 21% RH, 34% RH, 86% RH, 74% RH, and 30% RH for each day. Figure 4 shows the experimental location and the deployment of the observing equip-

Fig. 4. The diagram of field experiments including location and observation instrument.

ment, which included a DIAL lidar, a unmanned aerial vehicle (UAV) with an atmospheric monitoring system, and a micro-station with an ozone analyzer.

4.1. Verification experiment

The concentrated verification experiments were carried out using the atmospheric monitoring system and DIAL system on May 12th, 20th, 23th, 2022. Then, the DIAL system was optimized if the system offset was verified to exist and the value did not change from these experiments.

The UAV carried an airborne atmospheric monitoring system which was launched from a location approximately 2 m away from the lidar. The temporal resolution of the DIAL system is 10 minutes. One observation time of the UAV is approximately 30 minutes, thus the Lidar comparative data comes from the average of the three profiles. The UAV's flight speed and sampling frequency are not strictly uniform, and multiple hover observations are required at key heights. Therefore, these data need to be converted into a resolution of 7.5 m, which is consistent with the resolution for Lidar.

Two sets of typical comparative measurement profiles were selected from the continuous observation data for validation and analysis. These profiles are shown in Fig. 5. Figures 5(a) and (b) show ozone concentration profiles from the UAV and DIAL system on May 12th and 20th, respectively. The black profile represents the data obtained from the UAV, while the blue profile represents the original ozone concentration profile inferred by the Lidar. Other profiles represent the ozone concentration profiles retrieved by correcting the 289 nm backscattered signal offset at different values, respectively.

In Fig. 5, there is a larger gap between the original ozone concentration profile and the UAV data. The consistency has improved and the error has decreased due to correcting the 289 nm signal offset at a value of 7.5 m. However, there is still a big error between 150 and 450 m. The consistency is the best and the error is relatively small

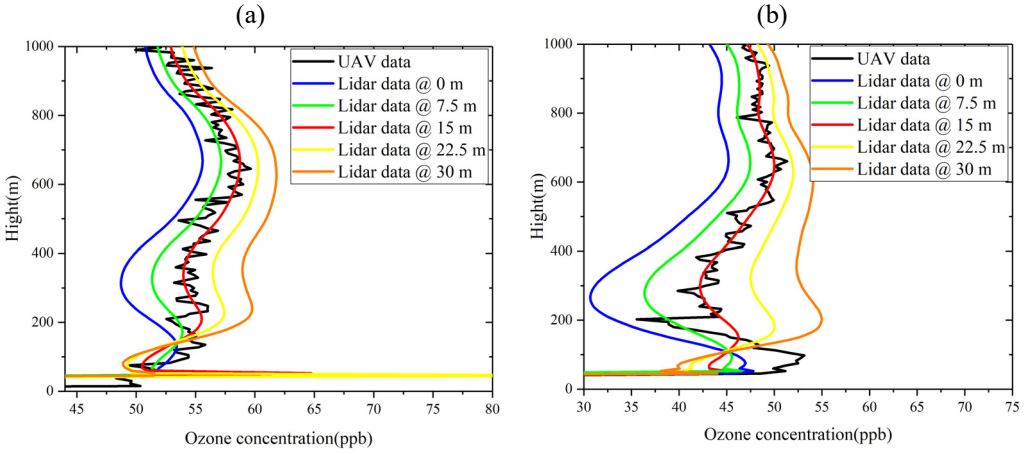

Fig. 5. Comparison of lidar and UAV data. (a) Experiment conducted on May 12th, 2022. (b) Experiment conducted on May 20th, 2022.

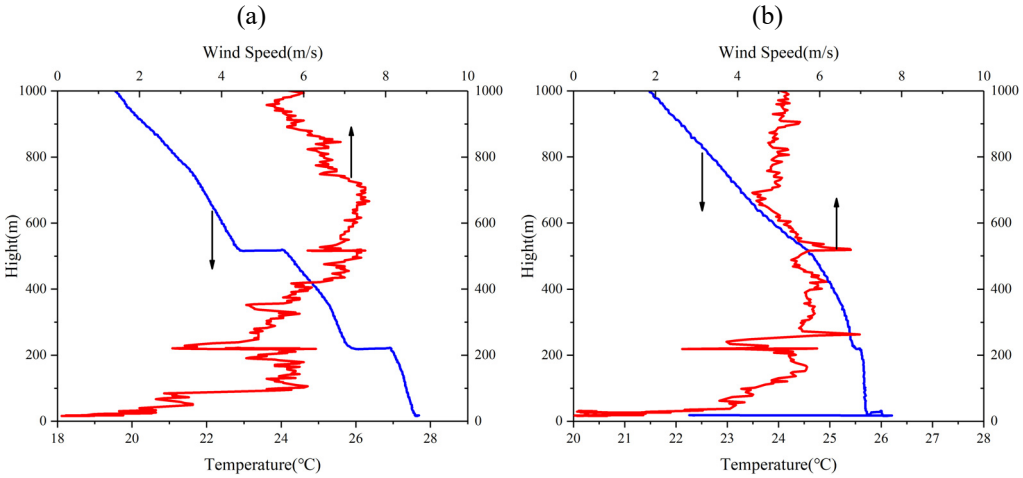

Fig. 6. Temperature and wind profile detected by UAV. (a) Experiment conducted on May 12th, 2022. (b) Experiment conducted on May 20th, 2022.

after correcting the 289 nm signal offset by 15 m. The consistency gradually deteriorates and the overall error becomes larger when the 289nm signal offset is corrected by 22.5 and 30 m. It is worth noting that the UAV data shows drastic changes at 200 and 500 m, which may be due to the existence of a boundary layer near these heights.

Figure 6 shows the temperature and wind speed data from 0 to 1000 m. It can be seen that there are sudden changes at heights of 200 and 500 m, where a boundary layer exists and the airflow is unstable.

Figure 7 shows the typical error curves from the experiments. The blue curve represents the original error between the UAV and DIAL. The black curve represents the error of the DIAL system corrected by deleting the 289 nm backscattered asynchronous

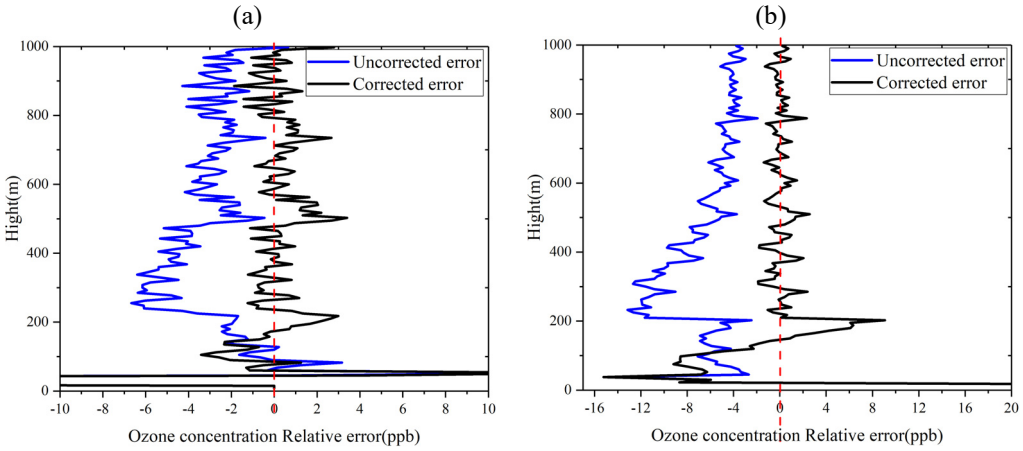

Fig. 7. Error curve for DIAL system. (a) Experiment conducted on May 12th, 2022. (b) Experiment conducted on May 20th, 2022.

offset. In Fig. 7, there is an offset in ozone concentration at all altitudes with a larger error closer to the ground. On May 12th, the maximum error in uncorrected data was 6.4 ppb corresponding to a height of 210 m, while 2 ppb corresponding to the height of 700 m after correction. On May 20th, the maximum error in uncorrected data was 13 ppb corresponding to a height of 300 m, while 2 ppb corresponded to the height of 800 m after correction. In addition, the error in corrected data was decreased obviously. The verification experiments show that the asynchronous offset in the DIAL system led to large errors in retrieval results. These errors have an inverse relationship with the detection range. The detection accuracy can be improved by reducing the asynchronous offset.

4.2. Reliability experiment

The continuous observation experiments were carried out with the DIAL system and the ozone analyzer as a reference, on May 20th–23th, 2022.

The ozone analyzer, which utilizes UV spectrophotometry with high accuracy, was installed in the Microstation about 10 m away from the DIAL. The key parameters of the analyzer are listed in Table 2.

T a b l e 2. Key parameters of ozone analyzer.

Items	Specification
Model	O342M
Measurement range	0–10
Accuracy	0.1 ppb
Power durability	60 min
Response time	20 s
Weight	9 kg
Dimension	$483 \times 545 \times 133$ mm^3
Work temperature	0–35°C

Because the DIAL has about a 50 m blind range, the data averaged from the height of 50 to 300 m was selected and compared with the ozone analyzer. The temporal resolution of the ozone analyzer is 1 minute, while the DIAL is 5 minutes. Hence, the five -date points from the analyzer should be averaged.

Figure 8 illustrated that the test data of the DIAL before moving out the offset (blue line) was less than the data from the analyzer (red line). There was a large error between the uncorrected data (blue line) and analyzer data (red line) with the maximum error of 29.1 ppb near 19:00 on May 21th, 2022. However, the corrected data from DIAL (black line) shows a relative improvement with the maximum error of 7.8 ppb near 17:00 on May 21th, 2022, and has good consistency with analyzer (red line). The detection accuracy of the improved DIAL has been further improved. It can be seen that there is poor consistency near 17:00 on 20th May. The reason is the humidity reached 90% RH, which affected the detection accuracy significantly. The reliability experi-

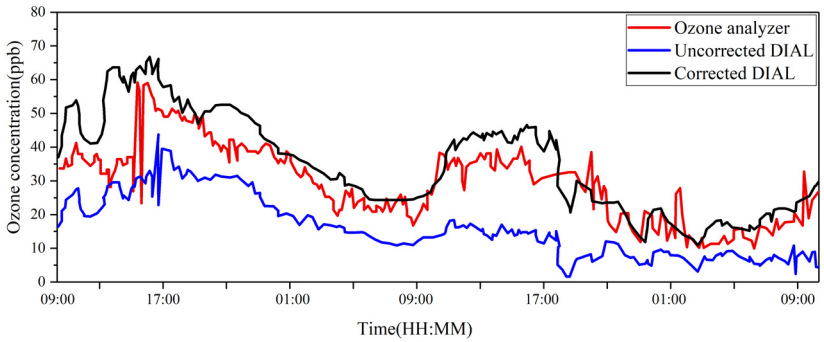

Fig. 8. Comparison measurements between the analyzer and the DIAL over 48 hours.

ment reveals that the optimized DIAL system has high stability during continuous observation. The trend consistency of improved DIAL is closer to that of fixed-point instruments. This optimized DIAL system can be used as another means to monitor the trend of ozone concentration at the ground, which expands the applications of ozone Lidar.

5. Conclusion

This study describes the ozone DIAL system utilized in both simulations and experiments, introducing a retrieval algorithm for measuring ozone concentration. Subsequently, numerical simulations analyzed the impact of asynchronous offset on the accuracy of DIAL detection. Simulation results indicate a direct correlation between the magnitude of asynchronous offset and the error in ozone retrieval. Under identical asynchronous offset conditions, a lower altitude corresponds to a greater error in ozone retrieval. Additionally, the presence of an asynchronous offset in the system exacerbates errors in ozone retrieval, especially during rapid ozone concentration changes. To validate the analytical findings, continuous observational experiments were conducted. The study proposes an optimization method aimed at enhancing the DIAL system's detection accuracy. To ascertain the optimization method's stability, the DIAL was operated continuously for 48 hours. Moreover, the enhanced DIAL system closely aligns with the ozone analyzer trends and can nearly substitute for the ozone analyzer in detecting near-surface ozone concentrations.

In our future research, we aim to enhance the DIAL system's detection accuracy further. To address the asynchronous offset, we intend to develop a cost-effective, high-precision acquisition card tailored for the DIAL system. Furthermore, we will conduct long-term field experiments to test the correction method's effectiveness and the system's stability across different weather conditions.

Acknowledgements

This work was supported by National and local joint engineering laboratory (NELCOF20210101); Natural Science Foundation of Anhui Provincial Higher Education (KJ2020A0128, KJ2021A0916, 2022AH052137,

2023AH051290); Sports Health Information Monitoring Technology Engineering Research Center (KF2023009); Information Materials and Intelligent Sensing Laboratory of Anhui Province (IMIS2021012). Authors are grateful for the continued support from our colleagues, collaborators, and friends. It is my pleasure to thank Dr. F. Han for his helpful comments on the paper especially.

References

[1] CHRISTIANSEN A., MICKLEY L.J., LIU J., OMAN L.D., HU L., *Multidecadal increases in global tropospheric ozone derived from ozonesonde and surface site observations: can models reproduce ozone trends?*, Atmospheric Chemistry and Physics **22**(22), 2022: 14751–14782. https://doi.org/10.5194/acp-22-14751-2022, 2022

[2] HONG J., WANG W., BAI Z., BIAN J., TAO M., KONOPKA P., PLOEGER F., MÜLLER R., WANG H., ZHANG J., ZHAO S., ZHU J., *The long-term trends and interannual variability in surface ozone levels in Beijing from 1995 to 2020*, Remote Sensing **14**(22), 2022: 5726. https://doi.org/10.3390/rs14225726

[3] PÉREZ A.B., DEVASTHALE A., BENDER F.A.-M., EKMAN A.M.L., *Impact of smoke and non-smoke aerosols on radiation and low-level clouds over the southeast Atlantic from co-located satellite observations*, Atmospheric Chemistry and Physics **21**(8), 2021: 6053-6077. https://doi.org/10.5194/acp-21-6053-2021

[4] ZAMAN S.U., PAVEL M.R.S., RANI R.I., JEBA F., ISLAM M.S., KHAN M.F., EDWARDS R., SALAM A., *Aerosol climatology characterization over Bangladesh using ground-based and remotely sensed satellite measurements*, Elementa: Science of the Anthropocene **10**(1), 2022: 000063. https://doi.org/10.1525/elementa.2021.000063

[5] KUANG S., WANG B., NEWCHURCH M., KNUPP K., TUCKER P., ELORANTA E., GARCIA J., RAZENKOV I., SULLIVAN J., BERKOFF T., GRONOFF G., LEI L., SENFF C., LANGFORD A., LEBLANC T., NATRAJ V., *Evaluation of UV aerosol retrievals from an ozone lidar*, Atmospheric Measurement Techniques **13**(10), 2020: 5277-5292. https://doi.org/10.5194/amt-13-5277-2020

[6] FAN G., LIU J., LIU W., LU Y., ZHANG T., DONG Y., ZHAO X., *A new retrieval method for ozone concentration at the troposphere based on differential absorption lidar*, Spectroscopy and Spectral Analysis **32**(12),2012: 3304-3308. https://doi.org/10.3964/j.issn.1000-0593(2012)12-3304-05

[7] PAPAYANNIS A., ANCELLET G., PELON J., MÉGIE G., *Multiwavelengh lidar for ozone measurements in the troposphere and the lower stratosphere*, Applied Optics **29**(4),1990: 467-476. https://doi.org/10.1364/AO.29.000467

[8] HU S., HU H., ZHOU J., WU Y., *Dual-differential LiDAR: a set of wavelengths that can improve the accuracy of ozone measurement*, Acta Meteorologica Sinica **60**(4), 2002: 486-493.

[9] CAO N., YANG F., SHI J., FUKUCHI T., *Noise effect on ozone DIAL night time measurement in the troposphere*, Acta Photonica Sinica **41**(12), 2012: 1416-1421. https://doi.org/10.3788/gzxb20124112.1416

[10] CHOUZA F., LEBLANC T., BREWER M., WANG P., *Upgrade and automation of the JPL Table Mountain Facility tropospheric ozone lidar (TMTOL) for near-ground ozone profiling and satellite validation*, Atmospheric Measurement Techniques **12**(1), 2019: 569-583. https://doi.org/10.5194/amt-12-569-2019

[11] KUANG S., NEWCHURCH M.J., BURRIS J., LIU X., *Ground-based lidar for atmospheric boundary layer ozone measurements*, Applied Optics **52**(15), 2013: 3557-3566. https://doi.org/10.1364/AO.52.003557

[12] LEBLANC T., SICA R., GIJSEL V., JOANNA A., HAEFELE A., PAYEN G., LIBERTI G., *Proposed standardized definitions for vertical resolution and uncertainty in the NDACC lidar ozone and temperature algorithms–Part 1: Vertical resolution*, Atmospheric Measurement Techniques **9**(8), 2016: 4029-4049. https://doi.org/10.5194/amt-9-4029-2016

[13] CHENG L., XIE C., ZHAO M., LI L., YANG H., FANG Z., CHEN J., LIU D., WANG Y., *Design of lidar data acquisition and control system in high repetition rate and photon-counting mode: Providing testing for space-borne lidar*, Sensors **22**(10), 2022: 3706. https://doi.org/10.3390/s22103706

[14] Liu R.L., Liu R.X., *Signal acquisition technology for photoelectric encoder based on FPGA*, Optik **127**(20), 2016: 9891-9895. https://doi.org/10.1016/j.ijleo.2016.07.082
[15] Liu P., Zhang T., Sun X., Fan G., Xiang Y., Fu Y., Dong Y., *Compact and movable ozone differential absorption lidar system based on an all-solid-state, tuning-free laser source*, Optics Express **28**(9), 2020: 13786-13800. https://doi.org/10.1364/OE.391333
[16] Kunz G.J., de Leeuw G., *Inversion of lidar signals with the slope mehod*, Applied Optics **32**(18), 1993: 3249-3255. https://doi.org/10.1364/AO.32.003249
[17] Weitkamp C., *Lidar: Range-Resolved Optical Remote Sensing of the Atmosphere*, Springer Series in Optical Sciences, Springer New York, NY, 2006. https://doi.org/10.1007/b106786
[18] U.S. Standard Atmosphere 1976, NOAA, 2015.

Received December 20, 2023
in revised form February 19, 2024